JME

*J*ournal of *M*ining & *E*nvironment,
Vol.8, No.3, 2017, 501-510.
DOI: 10.22044/jme.2017.953

A new method for 3-D magnetic data inversion with physical bound

M. Rezaie* and S. Moazam

Faculty of Engineering, Malayer University, Malayer, Iran

Received 31 December 2016; received in revised form 27 May 2017; accepted 13 June 2017
**Corresponding author: mohamad1rezaie@gmail.com (M. Rezaie).*

Abstract
Inversion of magnetic data is an important step towards interpretation of the practical data. Smooth inversion is a common technique for the inversion of data. Physical bound constraint can improve the solution to the magnetic inverse problem. However, how to introduce the bound constraint into the inversion procedure is important. Imposing bound constraint makes the magnetic data inversion a non-linear inverse problem. In this work, a new algorithm is developed for the 3D inversion of magnetic data, which uses an efficient penalization function for imposing the bound constraint and Gauss Newton method to achieve the solution. An adaptive regularization method is used in order to choose the regularization parameter in this inversion approach. The inversion results of synthetic data show that the new method can produce models that adequately match the real location and shape of the synthetic bodies. The test carried out on the field data from Mt. Milligan copper-gold porphyry deposit shows that the new inversion approach can produce the magnetic susceptibility models consistent with the true structures.

Keywords: *Magnetic Data, Inversion, Physical Bound, Gauss Newton, Regularization.*

1. Introduction

Magnetic surveys can provide useful information on the Earth's interior. Magnetic measurements are usually used to delineate magnetic anomalous bodies, and indicate their locations and depths. One of the most important topics in the quantitative interpretation of the potential field data is the inversion of practical data [1]. Inversion can be defined as a mathematical procedure that constructs a sub-surface property (susceptibility) model using the measured (magnetic) data by incorporating a-priori information as available. The recovered models must predict the measured data adequately [2]. 3D inversion of potential field data such as magnetic data is generally difficult [3]. The main difficulty is the non-uniqueness of the solution in magnetic inverse problem. There is infinite equivalent source distributions that produce the same measured magnetic data set [4]. In order to overcome this issue, the standard approach is to apply a-priori information. Several approaches have been introduced for incorporating priori information into the inversion process [5-15].

Last and Kubik (1983) [5] have developed the compact inversion method, which produces a compact and structurally simple model. Guillen and Menichetti (1984) [16] have minimized the moment of inertia of the body with respect to the center within the body or along the single axis passing through it. Barbosa and Silva (1994) [6] have generalized the moment of inertia functional to impose compactness along several axes. Li and Oldenburg (1996, 1998) [7, 8] have developed a model objective function that produces smooth models. This method can locate anomaly sources accurately. Nevertheless, the values for the recovered model are smaller than the true values due to the smoothness effect of the objective function. Portniaguine and Zhdanov (1999) [12] have developed a focusing inversion method based upon the compact inversion method for potential field data. Barbosa and Silva (2006) [17] have developed an interactive method for

inverting the magnetic data with interfering anomalies produced by multiple, complex, and closely separated geologic sources. Farquharson (2008) [13] has used the L1 measure of Li and Oldenburg's model objective function to recover dipping structures and models, which have angled interfaces. Lelievre et al. (2009) [14] have used the Li and Oldenburg's (1996, 1998) [7, 8] model objective function and developed advanced constrained inversion by geologic information. Zhang et al. (2015) [15] have improved the Li and Oldenburg's method by applying Lagrangian multipliers in the model objective function to add geological constraints. In the 3D inversion of potential field data, particular bounds of the physical property may be known. This physical bound constraint can improve the solution and make it more feasible [18]. Consequently, how to introduce the bound constraint into the inversion procedure becomes an important issue. Portniaguine and Zhdanov (1999, 2002) [12, 19] have used a penalization algorithm to impose bound constraint in focusing inversion of potential field data. Li and Oldenburg (2003) [9] have chosen a logarithmic barrier method incorporating bound constraint on the recovered smooth model. Zhang et al. (2015) [15] have imposed bound constraint in smooth inversion of potential field data via a method using the Lagrangian multipliers. However, imposing bound constraint makes the magnetic data inversion a non-linear inverse problem. Therefore, the logarithmic barrier and Lagrangian multiplier's methods increase the computation time. Another issue involved in solving the non-linear inverse problems is choosing the regularization parameter that can increase the computation time [20].

In this work, we developed a new 3D magnetic data inversion method based upon the Gauss-Newton (GN) algorithm that can incorporate bound constraint on the recovered model using penalization algorithm introduced by Portniaguine and Zhdanov (1999, 2002) [12, 19]. Furthermore, we used an adaptive regularization method for regularization parameter selection in our magnetic data inversion method. Finally, the capabilities of the proposed method were illustrated by its application to the inversion of a synthetic data set and to the 3D inversion of magnetic data from the Mt. Milligan deposit at British Columbia, Canada.

2. Methodology

2.1. Forward model for 3D magnetic anomalies

Susceptibility distribution in the sub-surface (κ) produces the magnetic field (T) at the surface. The purpose of the forward modeling is to compute this field. The total component of the magnetic field is given by [4]:

$$\vec{T} = -C_m \nabla \int_R \vec{m}.\nabla(\frac{1}{r})dv \quad (1)$$

where $C_m = 1\times10^{-7}$ (Henry.meter^{-1}), R denotes the volume occupied by the causative body, r is the distance, and $\vec{m}$ is the magnetization vector that can be obtained as follows:

$$\vec{m} = \kappa\vec{H} + \vec{m}_r \quad (2)$$

where $\vec{H}$ is the earth's magnetic field and $\vec{m}_r$ is remanent magnetization. If we ignore the remanent component, the magnetization will be in the direction of the earth's field, and can be obtained simply as:

$$\vec{m} = \kappa\vec{H} \quad (3)$$

To compute the total component of the magnetic field in Eq. (1), it is required to discrete the sub-surface under the survey area into rectangular prisms of known sizes and positions with constant susceptibilities. The formulation for computation of magnetic response for each rectangular prism was presented by Bhattacharyya (1964) [21] and later simplified into a form that is more suitable for fast computer implementation [22]. We used the formulation developed by Rao and Babu (1991) [22] to compute the magnetic response resulting from individual prisms. If the observed magnetic anomalies are caused by *M* subsurface prisms, the magnetic field at the field point *i* is given by:

$$T_i = \sum_{j=1}^{M} T_{i,j},\ i = 1,2,\ldots,N \quad (4)$$

where *N* is the number of observation point. The forward model of magnetic data using Eqs. (1) and (4) can be written as the following matrix equation:

$$\boldsymbol{T}_{N\times1} = G_{N\times M}\boldsymbol{\kappa}_{M\times1} \quad (5)$$

Here, *G* is the forward operator matrix that maps the physical parameter's space to the data space. $\boldsymbol{\kappa}$ denotes the vector of unknown model parameters and $\boldsymbol{T}$ is the data vector that is given by measurement data. There are some errors in the measurement data due to noise that is usually assumed to be uncorrelated, and have the Gaussian distribution [18]. Thus:

$$G\boldsymbol{\kappa} = \boldsymbol{d}^{obs} \tag{6}$$

where $\boldsymbol{d}^{obs} = \boldsymbol{T} + \boldsymbol{e}$ is the vector of the observed data and $\boldsymbol{e}_{N\times 1}$ is the vector of the data error. The main purpose of the magnetic inverse problem is to find a geologically plausible susceptibility model ($\boldsymbol{\kappa}$) based on G and some measured data ($\boldsymbol{d}^{obs}$) at the noise level.

2.2. Inversion method

In the typical minimum-structure inversion procedure, the sub-surface of the survey area is discrete into rectangular prisms (cells) of known sizes and positions with the values of the physical property (e.g. susceptibility) in the cells that are called the model parameters to be estimated in the inversion [1]. The solution can be obtained by minimization of an objective function, which is a combination of a measure of misfit between the observation and predicted data and a measure of complexity of the model subject to a physical bound constraint [7]:

$$\begin{aligned} &\Phi = \phi_d + \lambda\phi_\kappa \\ &s.t\ L \le \boldsymbol{\kappa} \le U \end{aligned} \tag{7}$$

where λ is a regularization parameter, L is the lower susceptibility bound, U is the upper susceptibility bound, and the misfit functional is defined as follows:

$$\phi_d = \left\| W_d(G\boldsymbol{\kappa} - \mathbf{d}^{obs}) \right\|_2^2 \tag{8}$$

Here, W_d is the data weighting matrix given by $W_d = diag(1/\sigma_i,...,1/\sigma_m)$, where σ_i stands for the standard deviation of the noise in the ith datum, and ϕ_κ is a stabilizing functional (stabilizer) that measures the minimum norm of model structure [7-9]:

$$\phi_\kappa = \boldsymbol{\kappa}^T(\sum_k \alpha_k W_k^T W_k)\boldsymbol{\kappa} \tag{9}$$

where α_k is the coefficient that affects the relative importance of derivative components in different directions. W_k resembles the first-order finite-difference matrices in the x, y, and z directions. We have to use an additional depth weighting matrix W_z for compensating the natural decay of the forward operator matrix with depth [23]:

$$W_z = diag(G^T G)^{1/4} \tag{10}$$

Now Eq. (9) can be reformulated to apply the depth weighting matrix to the objective function.

$$\phi_\kappa = \left\| W_m W_z \boldsymbol{\kappa} \right\|_2^2 \tag{11}$$

where W_m is the cumulative first-order finite-difference matrix. Eq. (7) can be reformulated easily using the matrix notation to incorporate depth weighting:

$$\Phi = \left\| \tilde{G} W_z^{-1} W_z \boldsymbol{\kappa} - \tilde{\mathbf{d}}^{obs} \right\|_2^2 + \lambda \left\| W_m W_z \boldsymbol{\kappa} \right\|_2^2 \tag{12}$$

where $\tilde{G} = W_d G$ and $\tilde{\mathbf{d}}^{obs} = W_d \mathbf{d}^{obs}$. Eq. (12) is transformed into a space of weighted model parameters $\boldsymbol{\kappa}_w$ by replacing the variables $\boldsymbol{\kappa} = W_z^{-1}\boldsymbol{\kappa}_w$ and $\tilde{G}_w = \tilde{G} W_z^{-1}$ [24]:

$$\Phi = \left\| \tilde{G}_w \boldsymbol{\kappa}_w - \tilde{\mathbf{d}}^{obs} \right\|_2^2 + \lambda \left\| W_m \boldsymbol{\kappa}_w \right\|_2^2 \tag{13}$$

The solution to Eq. (13) is obtained according to the regularization theory similar to the classical minimum norm optimization problem [25]. The solution to the magnetic inverse problem can be obtained by minimizing this equation using the GN method. The upper (U) and lower (L) susceptibility bounds can be imposed during the inversion process to recover a more feasible model. If an achieved susceptibility value falls outside the bounds, the value in that cell is projected back to the nearest upper or lower susceptibility bound [12].

In order to solve Eq. (13) with the GN method, assume the obtained solution denoted by $\boldsymbol{\kappa}_w^{(n-1)}$ at the (n − 1)th iteration, and the predicted data corresponding to this model is $\tilde{\mathbf{d}}^{(n-1)}$. Then at the nth iteration, a model perturbation $\Delta\boldsymbol{\kappa}_w$ can be achieved by solving the following equation so that the inverted model can be updated by $\boldsymbol{\kappa}_w^{(n)} = \boldsymbol{\kappa}_w^{(n-1)} + \Delta\boldsymbol{\kappa}_w$ [26]:

$$\begin{aligned} &(\tilde{G}_w^T \tilde{G}_w + \lambda^{(n)} \sum_k W_k^T W_k)\Delta\boldsymbol{\kappa}_w = \\ &\tilde{G}_w^T(\tilde{\mathbf{d}}^{obs} - \tilde{\mathbf{d}}^{(n-1)}) - \lambda^{(n)} \sum_k W_k^T W_k \boldsymbol{\kappa}_w^{(n-1)} \end{aligned} \tag{14}$$

where $\lambda^{(n)}$ is the regularization parameter in the nth iteration. Then the solution of the inverse problem in Eq. (7), $\boldsymbol{\kappa}$, is given by

$$\boldsymbol{\kappa}^{(n)} = \boldsymbol{\kappa}^{(n-1)} + W_z^{-1}\Delta\boldsymbol{\kappa}_w \quad (15)$$

In order to recover a more feasible model of the sub-surface, the upper (U) and lower (L) physical bounds of susceptibility are imposed in each iteration to force $L < \boldsymbol{\kappa}^{(n)} < U$. If a given susceptibility value falls outside the bounds, the susceptibility value of that cell is projected back to the nearest physical bound value.

The solution to Eq. (14) is also equivalent to the least-squares solution of the following equation:

$$\begin{bmatrix} \tilde{G}_w \\ \sqrt{\lambda^{(n)}}W_x \\ \sqrt{\lambda^{(n)}}W_y \\ \sqrt{\lambda^{(n)}}W_z \end{bmatrix} \Delta\boldsymbol{\kappa}_w = \begin{bmatrix} \tilde{\mathbf{d}}^{obs} - \tilde{\mathbf{d}}^{(n-1)} \\ -\sqrt{\lambda^{(n)}}W_x\boldsymbol{\kappa}_w^{(n-1)} \\ -\sqrt{\lambda^{(n)}}W_y\boldsymbol{\kappa}_w^{(n-1)} \\ -\sqrt{\lambda^{(n)}}W_z\boldsymbol{\kappa}_w^{(n-1)} \end{bmatrix} \quad (16)$$

The least-squares solution of Eq. (16) is obtained by a fast iterative method such as conjugate gradient (CG) [27] at each GN iteration. Therefore, the proposed algorithm would be suitable for the large-scale problems [18]. The GN iterations stop when the RMS misfit reaches an acceptable level or the model corrections become small enough [11].

We used an adaptive method for choosing the regularization parameter similar to what was proposed by Farquharson (2008) [13], which is a fast and efficient algorithm for choosing the regularization parameter. The regularization parameter is started at 100 ($\lambda^{(1)} = 100$), which is a relatively large value. If an inversion is performed with the regularization parameter fixed at this value, a model would be produced that has a small amount of structure and the predicted data under-fits the observations. At each iteration, the regularization parameter is damped to give a slow but steady progression of models with increasing structure and decreasing data misfits:

$$\lambda^{(n)} = \lambda^{(1)}\theta^{n-1}, \quad n = 1,2,\ldots \quad (17)$$

where $\theta = 0.5$ based on the empirical experiments.

3. Synthetic test

We applied our algorithm to two synthetic tests in order to evaluate the reliability of the introduced method. The first synthetic model consisted of two different blocks with the dimension 200 m × 200 m × 200 m, which was embedded below the surface so that the susceptibility of uniform background was zero. The susceptibility of each block was 0.06 (SI). The perspective view of the true model is displayed in Figure 1a.

The depth to the top of the shallower block (block (1)) was 50 m, and the depth above the top of the deeper block (block (2)) was 100 m. The total-field anomaly data was generated at the surface assuming an inducing field with inclination (I) of 75°, declination (D) of 25°, and a strength of 50000 nT. The data was generated over a grid of 1000 m × 1000 m with a sample spacing of 25 m. There was 1600 data, and 5% Gaussian noise of the accurate datum magnitude was added (Figure 1b). The sub-surface was divided into 40 × 40 × 20 = 32000 rectangular prisms with the same size of 25 m for inversion. The inverse problem was solved using the proposed method that was described in the preceding section ($\alpha_1 = \alpha_2 = \alpha_3 = 1$). The solution was obtained after five iterations with an RMS of 0.05.

Figure 2 shows a plan section and a cross-section through the recovered model from proposed inversion method. The result indicates an acceptable smooth reconstruction of the synthetic multi-source blocks at different depth levels below the surface. The recovered bodies in the model are smooth and adequately match the real location of synthetic bodies.

The second synthetic model is more complicated and consists of two 3D dipping slabs buried in a zero susceptibility half-space (earth). The susceptibility of both slabs was 0.06 (SI). The perspective view of the true model is displayed in Figure 3a.

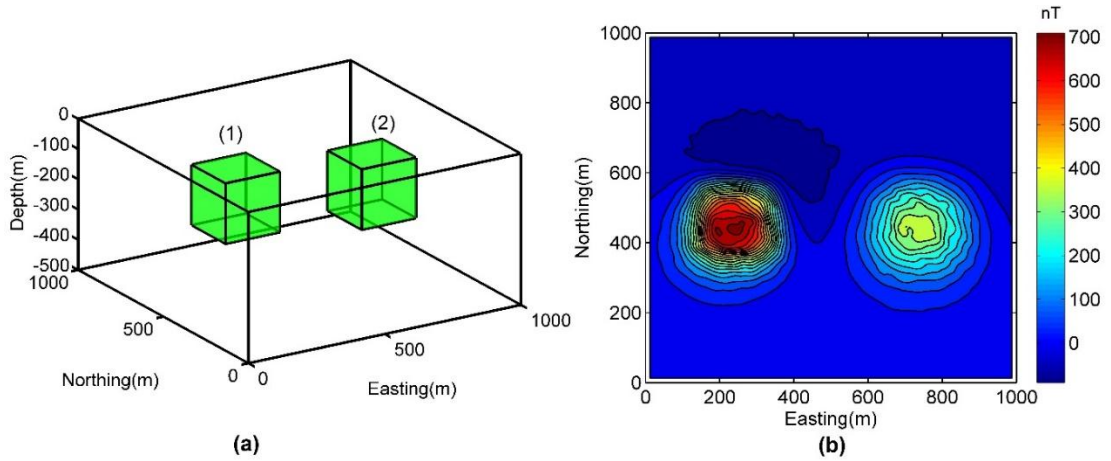

Figure 1. Perspective view of first synthetic model with two blocks (a). Magnetic anomaly was produced by first synthetic model with 5% Gaussian noise of accurate datum magnitude.

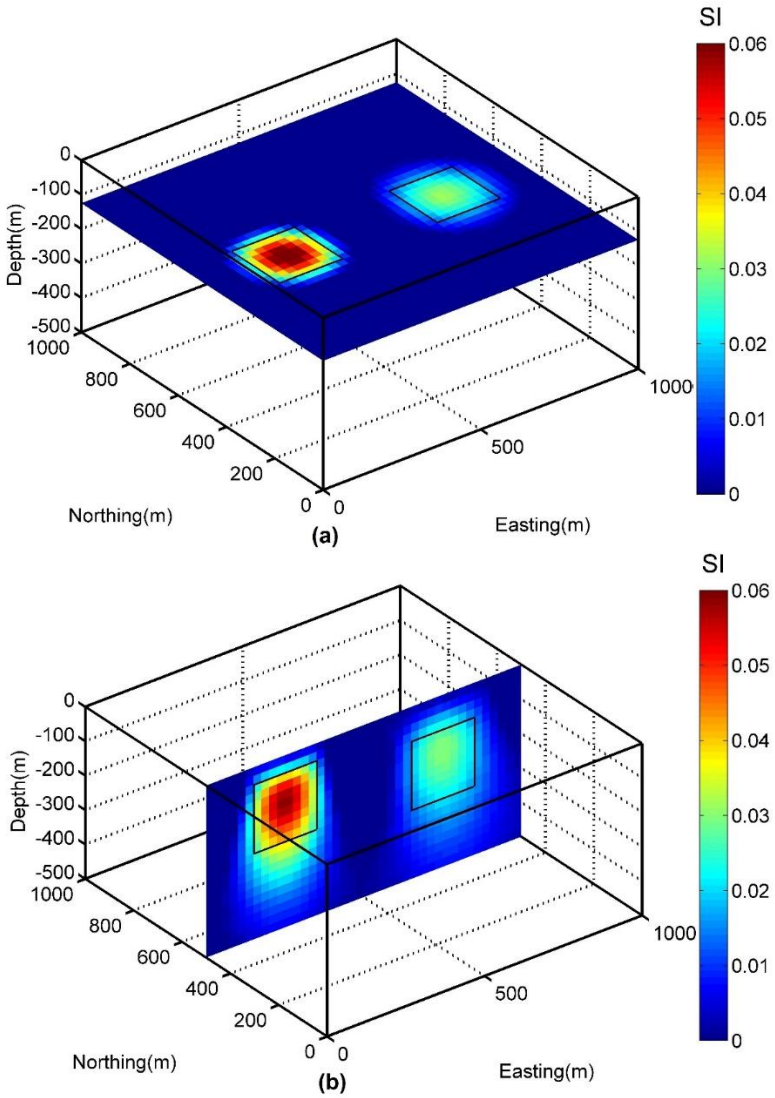

Figure 2. Plan sections through recovered susceptibility model obtained from 3D inversion of magnetic data from first synthetic model at depth = -125 m (a). A cross-sectional slice of susceptibility model at Northing = 500 m (b). Borders indicate true position of each body.

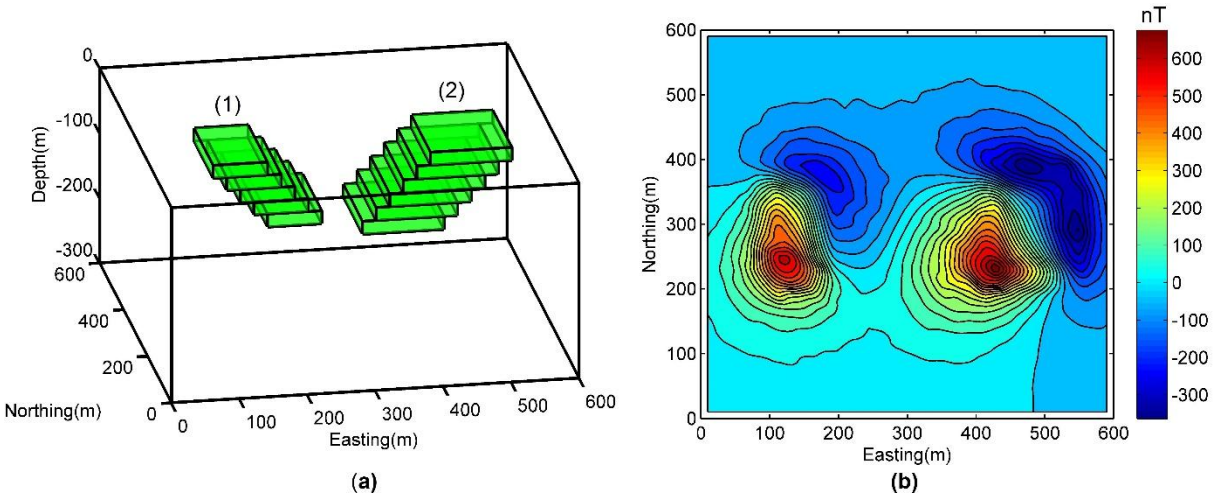

Figure 3. Perspective view of second synthetic model with two dipping slabs (a). Magnetic anomaly was produced by second synthetic model with 5% Gaussian noise of accurate datum magnitude.

The depth to the top was 20 m for both dipping slabs. Slab (1) elongated to 120 m below the surface, and its thickness was 80 m in the east direction. The second slab elongated 140 m below the surface, and its thickness was 120 m in the east direction. The length of both dipping slabs was 160 m, which elongated in the north direction. Under an inducing field of a strength of 48000 nT, inclination (I) of 45°, and declination (D) of 45°, the synthetic model produced 900 surface total magnetic data. 5% Gaussian noise of the accurate datum magnitude was added to the data (Figure 3b). The data was generated over a grid of 600 m × 600 m with a sample spacing of 20 m.

The sub-surface was discretized into 30 × 30 × 15 = 13500 rectangular prisms with the same size of 20 m for inversion. The inverse problem was solved using the proposed method ($\alpha_1 = \alpha_2 = \alpha_3 = 1$). The solution was obtained after 73 iterations with RMS of 0.05.

Figure 4 shows a plan section and a cross-section through the recovered model from the proposed inversion method. The anomalous bodies in the model were smooth, and the tabular shape of the slabs and their dipping structure were clear. The depth extents of the slabs were reasonably recovered. The susceptibility amplitude of the recovered model was slightly lesser than the true value at the lower corner of slabs in dipping directions but the dip angles inferred from the recovered model were close to the true value. However, the result indicates acceptable smooth reconstruction of the synthetic multi-source slabs at different depth levels below the surface.

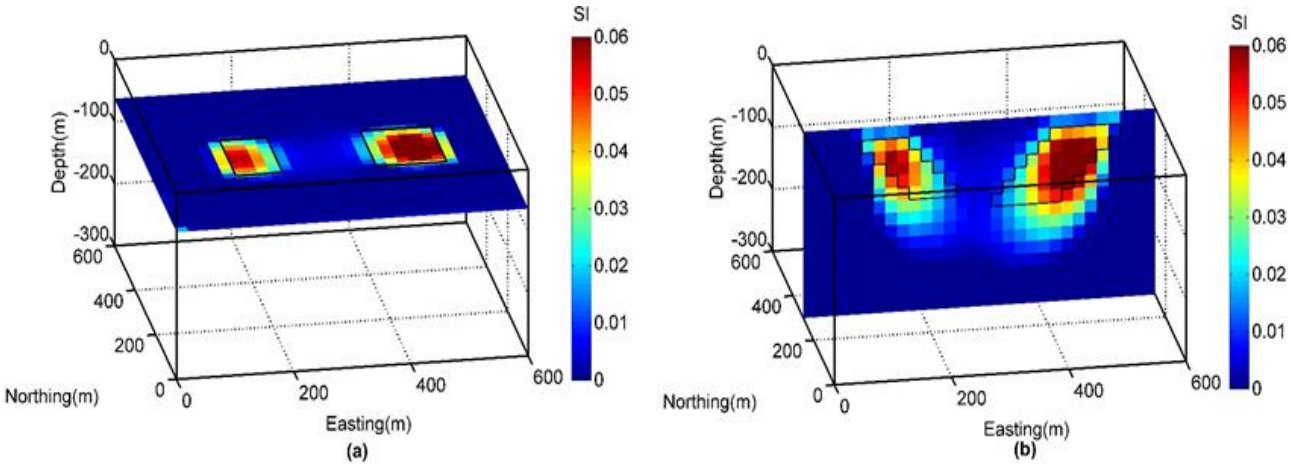

Figure 4. Plan sections through recovered susceptibility model obtained from 3D inversion of magnetic data form second synthetic model at depth = -60 m (a). A cross-sectional slice of susceptibility model at Northing = 300 m (b). Borders indicate true position of each slab.

4. Inversion of field data

Mt. Milligan is a copper-gold porphyry deposit situated in central British Columbia. The geological information obtained from a major drilling program show that the host rocks of the deposit are Mesozoic volcanic and sedimentary rocks, and contain intrusive monzonitic rocks that have accessory magnetite. There is an intensive hydrothermal alteration primarily in the region beyond the boundaries of the monzonite stock. The monzonite body is known as the MBX stock [28]. Copper and gold are concentrated in the potassic alteration zone, which is mainly around the contact of the monzonite intrusions (MBX) and may extend outward and into the fractured volcanic rocks. However, magnetite is one of the strong indicators of the potassic alteration. In this region, the magnetic data is acquired at 12.5 m spacing along lines in the east direction that spaced 50 m apart [7]. We used the data at 25 m spacing, which yields 1920 data point. The reduced magnetic anomaly map is shown in Figure 5.

The direction of the inducing field is I = 75° and D = 25.73° with a strength of 58193 nT. It is assumed that each datum has an error whose standard deviation is equal to 5% of its magnitude [9].

In order to invert this data, the sub-surface of the area was discretized into 48 × 40 × 18 = 34560 cells, each of size 25 m. The positivity constraint was imposed, which means that the lower (L) physical bounds of susceptibility are set to 0 SI. The solution is obtained after 112 iterations with an RMS error of 0.05, which is about the predicted noise of the data. The recovered model is shown in Figure 6 as one plan-section and one cross-section. The true edge of the MBX stock and mineral assemblage, which were derived from the drilling results overlaid on the cross-section of the recovered susceptibility model (Figure 6b).

The results obtained indicate that the anomalous bodies of magnetic susceptibility highs are mostly associated with the monzonite intrusion (MBX or black polygon in Figure 6b). There is a moderate anomalous body at the center of the cross-section, which is probably caused by the magnetite content of potassic alteration. This area coincides with mineral deposit (red-shaded polygon in Figure 6b). Thus the solution obtained is in a good agreement with the true geologic boundaries of Mt. Milligan deposit (Figure 6b).

The results obtained from the presented algorithm are virtually similar with the ones obtained by Li and Oldenburg (2003) [9]. Figure 7 shows a cross-section through the model obtained by Li and Oldenburg (2003) [9] at the northing of 600 m.

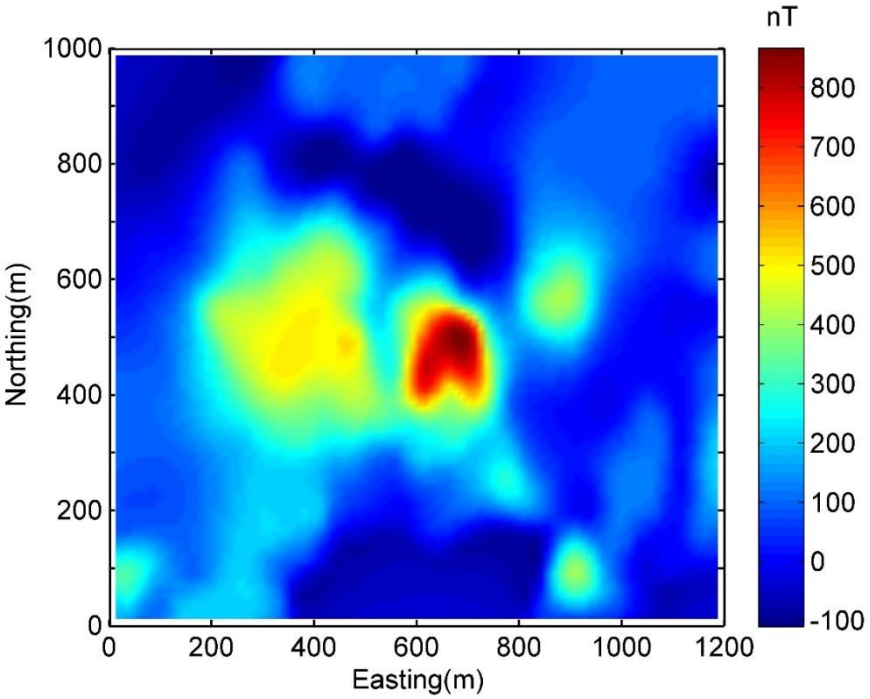

Figure 5. Magnetic anomaly map of Mt. Milligan. Data is on 25 m × 25 m grid.

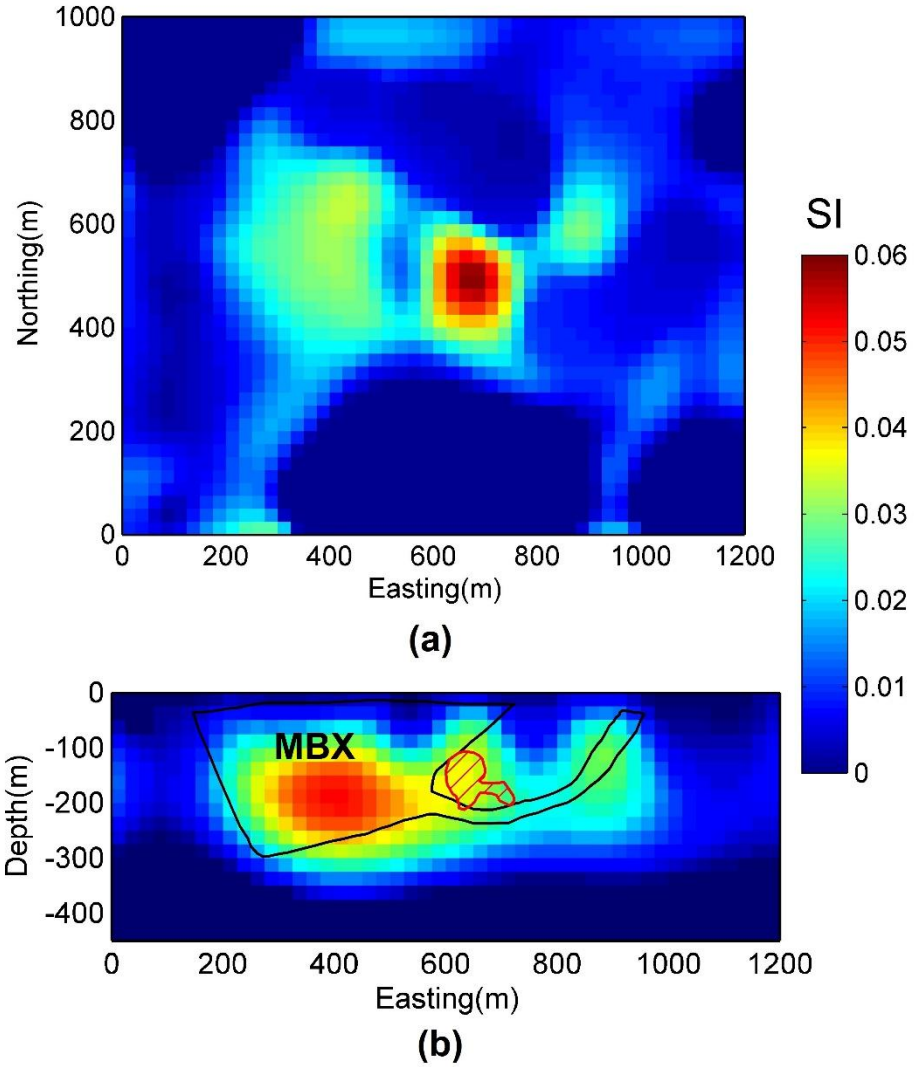

Figure 6. Recovered susceptibility model shown in a plan-section at a depth of -80 m (a). A cross-section at northing of 600 m overlaid by true boundary of monzonite body (MBX) with black line and mineral deposit with red-shaded polygon (b).

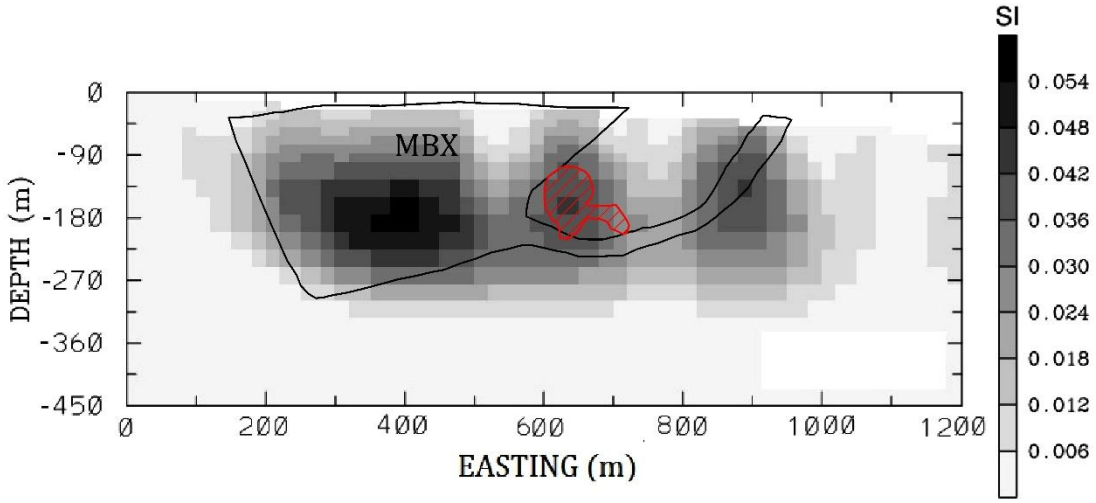

Figure 7. A cross-section through model obtained by Li and Oldenburg (2003) [9] at northing of 600 m overlaid by true boundary of monzonite body (MBX) with black line and mineral deposit with red-shaded polygon (after [9]).

5. Conclusions

We developed a new algorithm for inversion of magnetic data using the Gauss Newton method. In each GN iteration, the CG method is used for solving the least-square problem. Therefore, the proposed algorithm is efficient for large-scale problems. We used an adaptive regularization method for choosing the regularization parameter in each iteration, which is a fast and effective method for choosing the regularization parameter. In the new algorithm, the physical bound constraint can be imposed during the inversion process via penalization function, which does not require any transformation. Consequently, this method of imposing bound constraint is more efficient.

The results obtained show that the new developed 3D inversion method can produce a smooth solution, which defines the shape and extent of synthetic bodies adequately. Furthermore, this inversion algorithm has been applied for inversion of a field magnetic data from Mt. Milligan deposit. It produced a model that is consistent with the available geological information of the deposit.

Compression methods such as wavelet compression that can compress the kernel matrix and using parallel programming that decrease the required memory and computation time will be the subject for future works for large-scale problems.

References

[1]. Rezaie, M., Moradzadeh, A. and Kalate, A.N. (2017). 3D gravity data-space inversion with sparseness and bound constraints. J. Min. Environ. 8 (2): 227-235.

[2]. Foks, N.L., Krahenbuhl, R. and Li, Y. (2014). Adaptive sampling of potential-field data : A direct approach to compressive inversion. Geophysics. 79 (1): IM1-IM9.

[3]. Jin, S.G., van Dam, T. and Wdowinski, S. (2013). Observing and understanding the Earth system variations from space geodesy. J. Geodyn. 72: 1-10.

[4]. Blakely, R.J. (1996). Potential theory in gravity and magnetic applications. Cambridge University Press. Cambridge, 441 P.

[5]. Last, B.J. and Kubik, K. (1983). Compact gravity inversion. Geophysics. 48: 713-721.

[6]. Barbosa, V.C.F. and Silva, J.B.C. (1994). Generalized compact gravity inversion. Geophysics. 59: 57- 68.

[7]. Li, Y. and Oldenburg, D.W. (1996). 3-D inversion of magnetic data. Geophysics. 61 (2): 394-408.

[8]. Li, Y. and Oldenburg, D.W. (1998). 3-D inversion of gravity data. Geophysics. 63 (1): 109-119.

[9]. Li, Y. and Oldenburg, D.W. (2003). Fast inversion of large-scale magnetic data using wavelet transforms and a logarithmic barrier method. Geophys. J. Int. 152 (2): 251-265.

[10]. Pilkington, M. (1997). 3-D magnetic imaging using conjugate gradients. Geophysics. 62 (4): 1132-1142.

[11]. Pilkington, M. (2008). 3D magnetic data-space inversion with sparseness constraints. Geophysics. 74 (1): L7-L15.

[12]. Portniaguine O. and Zhdanov, M.S. (1999). Focusing geophysical inversion images. Geophysics. 64: 874-887.

[13]. Farquharson, C.G. (2008). Constructing piecewise-constant models in multidimensional minimum-structure inversions. Geophysics. 73 (1): K1-K9.

[14]. Lelièvre, P.G., Oldenburg, D.W. and Williams, N.C. (2009). Integrating geological and geophysical data through advanced constrained inversions. Explor. Geophys. 40 (4): 334-341.

[15]. Zhang, Y., Yan, J., Li, F., Chen, C., Mei, B., Jin, S. and Dohm, J.H. (2015). A new bound constraints method for 3-D potential field data inversion using Lagrangian multipliers. Geophys. J. Int. 201 (1): 267-275.

[16]. Guillen, A. and Menichetti, V. (1984). Gravity and magnetic inversion with minimization of a specific functional. Geophysics. 49: 1354-1360.

[17]. Barbosa, V.C.F. and Silva, J.B.C. (2006). Interactive 2D magnetic inversion: A tool for aiding forward modeling and testing geologic hypotheses. Geophysics. 71 (5): L43-L50.

[18]. Rezaie, M., Moradzadeh, A., Kalate, A.N. and Aghajani, H. (2017). Fast 3D Focusing Inversion of Gravity Data Using Reweighted Regularized Lanczos Bidiagonalization Method. Pure. Appl. Geophys. 174: 359-374.

[19]. Portniaguine, O. and Zhdanov, M.S. (2002). 3-D magnetic inversion with data compression and image focusing. Geophysics. 67 (5): 1532-1541.

[20]. Farquharson, C.G. and Oldenburg, D.W. (2004). A comparison of automatic techniques for estimating the regularization parameter in non-linear inverse problems. Geophys. J. Int. 156 (3): 411-425.

[21]. Bhattacharyya, B.K. (1964). Magnetic anomalies due to prism-shaped bodies with arbitrary polarization. Geophysics. 29 (4): 517-531.

[22]. Rao, D.B. and Babu, N.R. (1991). A rapid method for three-dimensional modeling of magnetic anomalies. Geophysics. 56 (11): 1729-1737.

[23]. Zhdanov, M.S. (2015). Inverse theory and applications in geophysics. Vol. 36. Elsevier. 704 P.

[24]. Rezaie, M., Moradzadeh, A. and Kalateh, A.N. (2017). Fast 3D inversion of gravity data using solution space priorconditioned lanczos bidiagonalization. J. Appl. Geophys. 136: 42-50.

[25]. Tikhonov, A.N., Arsenin, V.I. and John, F. (1977). Solutions of ill-posed problems. Vh Winston. Washington DC. 258 P.

[26]. Aster, R.C., Borchers, B. and Thurber, C.H. (2013). Parameter estimation and inverse problems. Elsevier Academic. 360 P.

[27]. Hestenes, M.R. and Stiefel, E. (1952). Methods of conjugate gradients for solving linear systems. J. Res. Natl. Bur. Stand. 49 (6): 409-436.

[28]. Oldenburg, D.W., Li, Y. and Ellis, R.G. (1997). Inversion of geophysical data over a copper gold porphyry deposit: A case history for Mt. Milligan. Geophysics. 62 (5): 1419-1431.

روشی جدید برای مدل‌سازی وارون سه‌بعدی داده‌های مغناطیس با قید کران فیزیکی

محمد رضایی* و سحر معظم

دانشکده فنی و مهندسی، دانشگاه ملایر، ایران

ارسال ۲۰۱۶/۱۲/۳۱، پذیرش ۲۰۱۷/۶/۱۳

* نویسنده مسئول مکاتبات: mohamad1rezaie@gmail.com

چکیده:

مدل‌سازی وارون داده‌های مغناطیس گامی است مهم برای تفسیر این داده‌ها. مدل‌سازی وارون هموار، روشی است رایج برای مدل‌سازی وارون این داده‌ها. اعمال قید کران فیزیکی می‌تواند جواب مسئله وارون مغناطیس را بهبود ببخشد. به هر حال نحوه اعمال قید کران در فرآیند مدل‌سازی وارون مهم است. اعمال قید کران مسئله مدل‌سازی وارون داده‌های مغناطیس را به یک مسئله وارون غیرخطی تبدیل می‌کند. در این پژوهش، الگوریتم جدیدی برای مدل‌سازی سه‌بعدی داده‌های مغناطیس توسعه داده می‌شود که در آن از یک تابع مجازات کارا برای اعمال قید کران به کار گرفته شده است و از روش گوس نیوتن برای رسیدن به جواب استفاده شده است. در این روش مدل‌سازی وارون، یک روش منظم‌سازی تطبیقی برای انتخاب پارامتر منظم‌سازی به کار گرفته شده است. مدل‌سازی وارون داده‌های مصنوعی نشان می‌دهد که این روش جدید می‌تواند شکل و محل واقعی توده‌های موجود در مدل مصنوعی را به خوبی مشخص کند. آزمایش انجام شده با استفاده از داده‌های میدانی ذخیره مس- طلای پرفیری کوه میلیگان نشان می‌دهد که روش جدید مدل‌سازی وارون می‌تواند مدل‌هایی برای توزیع خودپذیری مغناطیسی تهیه کنند به گونه‌ای که با ساختارهای واقعی زمین همخوانی دارد.

کلمات کلیدی: داده‌های مغناطیس، مدل‌سازی وارون، قید کران فیزیکی، گوس نیوتن، منظم‌سازی.